Fast synthesis of n-type half-heusler TiNiSn thermoelectric material

Fast Synthesis of n-Type Half-Heusler TiNiSn Thermoelectric Material

Kan Chen[1,*], Chris Nuttall[2], Eleni Stefanaki[3], Katarzyna Placha[3], Richard Tuley[3], Kevin Simpson[3], Jan-Willem G. Bos[4], Michael J Reece[1]

[1]School of Engineering and Materials Science, Queen Mary University of London, Mile End Road, London E1 4NS, UK.

[2]Johnson Matthey Technology Centre, Blounts Court Road, RG4 9NH, Sonning Common, UK

[3]European Thermodynamics Ltd., 8 Priory Business Park, Wistow Road, Kibworth, LE8 0R, UK

[4]Institute of Chemical Sciences and Centre for Advanced Energy Storage and Recovery, School of Engineering and Physical Sciences, Heriot-Watt University, Edinburgh, EH14 4AS, UK

*Corresponding author at: School of Engineering and Materials Science, Queen Mary University of London, London, E1 4NS, UK. E-mail addresses: kan.chen@qmul.ac.uk

Abstract

The n-type half-Heusler TiNiSn is very promising for thermoelectric applications in the medium temperature range. However, the synthesis of TiNiSn often involves long annealing times (up to several weeks) to obtain single phase, which is a major barrier to scaling-up. In this work, TiNiSn was synthesized by a combination of arc-melting, ball-milling and spark plasma sintering. The obtained samples with diameters up to 30 mm had high-purity, high-density and fine-grains. Without the need for an annealing step, the total synthesis time was significantly shortened. Addition of Cu was used to optimize the thermoelectric properties of TiNiSn, and a maximum figure of merit of 0.6 was achieved at 773 K. The fast and scalable synthesis of TiNiSn with good thermoelectric performance presented in this work opens up the possibility of industrial scaling-up.

Keywords

Thermoelectric materials; Heusler phases; synthesis; joining; aging.

Thermoelectric (TE) generators have great potential for energy harvesting from waste heat. The conversion efficiency of a TE generator is dominated by the dimensionless figure-of-merit defined as $zT = \alpha^2\rho^{-1}\kappa^{-1}T$, where α is the Seebeck coefficient, ρ is the electrical resistivity, κ is the thermal conductivity and T is the absolute temperature [1, 2]. An ideal thermoelectric material should have a high power factor ($\alpha^2\rho^{-1}$) to give a high power output from the TE generator and a low thermal conductivity (κ) to maintain a temperature gradient and reduce conduction heat losses [3]. The n-type Half-Heusler (HH) compound TiNiSn is of considerable interest for TE generators operating with a hot-side in the 700 K to 900 K temperature regime, due to its excellent electrical transport properties, good mechanical properties and stability, low-cost and low-toxicity [4-6]. However, it is challenging to obtain high-purity TiNiSn due to the fact that the constituent elements have very different melting points (Ti, 1943 K; Ni, 1728 K; Sn, 505 K.) and there are competitive full-Heusler $TiNi_2Sn$ and intermetallic binary phases [7]. Conventionally, TiNiSn is prepared via a solid-state method in sealed quartz tubes or by arc-melting or induction melting, followed by an additional annealing process in sealed quartz tubes for up to several weeks [5, 8-10]. This conventional method is time and energy consuming, which is a barrier to scaling-up. There have been attempts using other methods to prepare TiNiSn. Karati et al. reported using mechanically activated annealing to prepare TiNiSn powder, and the annealing time was reduced to 2h [11]. However, the sample still had an impurity of $TiNi_2Sn$ and the thermoelectric performance was not

reported. Birkel et al. reported using microwave processing combined with hot-pressing to prepare TiNiSn, but the sample after hot-pressing had obvious impurities and was inhomogeneous [12]. Ball-milling (BM) is a widely used synthesis method for alloys, but it was reported that TiNiSn cannot be synthesized directly by BM, even with a prolonged milling time of up to 20 h, due to the easy formation of Ni_3Sn_4 [13, 14]. Recently, Tillard et al. readdressed the problem with TiNiSn prepared by BM and revealed that an optimal energy window exists for direct formation of TiNiSn by BM. TiNiSn phase can be formed with a milling speed of 500 rpm for 5h [15]. The optimum conditions do not always correspond to higher milling speed and longer milling time, and TiNiSn will decompose if the energy provided by BM is too high. However, they concluded it is not possible to unambiguously confirm the phase based on the XRD of ball-milled powder, as peak broadening could mask other phases such as $TiNi_2Sn$, and there was no further investigation of the densified TiNiSn in their work. It is difficult to directly synthesis high-purity TiNiSn by BM, but it can provide enough energy for the formation of the TiNiSn phase from the precursor elements. In the current work we investigated the combination of arc-melting (AM) followed by BM to produce high purity TiNiSn powder, which was then densified by spark plasma sintering (SPS), thus avoiding the need for long annealing times. With optimized BM and SPS conditions, well crystallized, high-density and high-purity TiNiSn samples were obtained. The thermoelectric properties of TiNiSn with different levels of Cu doping were investigated, and

the results are consistent with previous work on $TiNiCu_xSn$ prepared by the conventional method involving long annealing times [5]. In addition, we also produced large samples of 30 mm diameter with optimal composition of $TiNiCu_{0.05}Sn$ and confirmed its homogeneity and thermoelectric performance. Preliminary joining and thermal aging tests indicate a low electrical contact resistance can be achieved in $TiNiCu_{0.05}Sn$ sample with good stability.

Polycrystalline $TiNiCu_xSn$ (x = 0, 0.05, 0.1, 0.15 and 0.2) samples were prepared by AM + BM + SPS. Starting materials of Ti, Ni, Cu and Sn wires (1.0 mm dia, > 99.98 %, AlfaAesar) were weighed according to the required stoichiometric ratios and arc-melted in a glove box. The arc-melted ingots were flipped and remelted three times to improve their homogeneity. The obtained ingots were crushed and ball-milled under optimised conditions; in argon at a rotation speed of 300 rpm for 200 min in a planetary ball mill machine (PULVERISETTE 5/4, Fritsch). The ball-milled powders were sintered at 973 K, 50 MPa for 5 min using a SPS furnace (FCT HPD 25). Both Φ15 mm and Φ 30 mm samples were sintered. The phases of the samples were examined using X-ray powder diffraction (XRD, PANalytical X'Pert Pro, CuKα). The microstructures and compositions were investigated using scanning electron microscopy (SEM, FEI, Inspect F, 10 kV). Secondary electrons images were taken of freshly fractured surfaces, while backscattered electron images and energy-dispersive X-ray spectroscopy (EDX) mapping was performed on polished surfaces. The electrical

resistivity and Seebeck coefficient were measured in the direction perpendicular to the SPS pressing direction using a commercial instrument (LSR-3/110, Linseis) in a He atmosphere up to 773 K. The uncertainty of the resistivity and Seebeck coefficient values is less than 5%. The thermal diffusivity was measured in the direction parallel to the SPS pressing direction using the flash diffusivity method (LFA 457, Netzsch) up to 773 K. The specific heat capacity (C_p) was estimated using the Dulong-Petit law. The uncertainty of thermal diffusivity measurements is less than 5 %. The density was measured using the Archimedes method and the results are provided in Table S1. The thermal conductivity was calculated using the thermal diffusivity, specific heat capacity and density.

Figure 1(a) shows the XRD patterns of the TiNiSn materials after AM, BM and the $TiNiCu_xSn$ samples after SPS. After AM, TiNiSn was the main phase, but there were obvious impurities of $TiNi_2Sn$, Ti_6Sn_5, Sn and some unidentified phases. The formation of impurities was inevitable due to the fast cooling from liquid state during the AM process [15]. Then the AM ingot was crushed and ball-milled using optimized conditions. From the XRD of TiNiSn after BM, it can be seen that the impurities were eliminated. However, the XRD peaks are broad, and it is possible that there might have still been some $TiNi_2Sn$ present due to the fact that it has very similar crystal structure and lattice parameter as TiNiSn. The phase purity was confirmed after SPS; the sample was well crystallized with sharp peaks, all of which were indexed as TiNiSn (PDF: 03-

065-0617). There were no observable impurities within the detection limit of XRD. The results indicate that BM was effective in eliminating any impurities in the sample after AM. The synthesis method of AM+BM developed in this work takes less than 5 h, which is much more time efficient than the conventional annealing process (typically 2 weeks). Additionally, a lower milling speed and shorter milling time are required than those reported for the direct formation of TiNiSn by BM (5h to 20h) [14, 15]. When optimizing the BM conditions, we noticed that longer milling times resulted in the reappearance of the $TiNi_2Sn$ impurity (See Figure S1), which is consistent with Tillard et al.'s work [15]. This indicates that the XRD peak broadening can cover the existence of $TiNi_2Sn$ in the sample after BM, which is worth noting when considering the discussion of the XRD results for other HH compounds prepared by BM. The $TiNiCu_xSn$ samples were single phase for $x \leq 0.1$, and for the $x = 0.15$ and 0.2 samples a second phase of $TiNi_2Sn$ was formed. The calculated lattice parameters of the $TiNiCu_xSn$ samples after SPS are shown in Figure 1(b), which shows that Cu is accommodated within the TiNiSn matrix, causing an expansion of the lattice parameter until the secondary $TiNi_2Sn$ phase forms. These results are consistent with a previous report [5].

Figure 2(a) shows a typical fracture surface of a representative sample of $TiNiCu_{0.1}Sn$. The samples were dense and well-crystallised with sub-micron grains. The grain size was much smaller than that reported for a sample prepared

by a combination of conventional solid-state reaction, annealing and hot-pressing, which had a grain size of 2 ~ 5 μm [5]. The small grains, produced by the BM and fast sintering of SPS, are favourable for realizing low thermal conductivity. To investigate the phase purity and homogeneity, backscattered electron images and corresponding EDX maps were taken of polished surfaces, as shown in Figure 2(b) and 2(c). No obvious impurities were observed and the elemental distribution was apparently homogeneous. These results further confirm that the processing route of AM + BM + SPS adopted in this work can produce TiNiSn samples with high density, high purity and fine grain size.

The temperature dependent thermoelectric properties of $TiNiCu_xSn$ are shown in Figure 3. All of the samples had a negative Seebeck coefficient, indicating they had n-type charge carriers. The undoped TiNiSn sample showed semiconducting behavior with a relatively large electrical resistivity that decreased with increasing temperature. The absolute value of Seebeck coefficient of the undoped TiNiSn sample first increased with increasing temperature as the absolute value of Seebeck coefficient is proportional to temperature, and then it decreased with increasing temperature due to the bipolar effect. The additional Cu significantly reduced the resistivity over the entire measurement temperature range, and the samples showed metal-like behavior as the electrical resistivity increased with increasing temperature. With increasing Cu content, the resistivity was further reduced, while the absolute value of Seebeck coefficient decreased accordingly.

This indicates that the additional Cu effectively worked as an n-type dopant. The power factor was enhanced, and a maximum power factor of 3.1 $mWK^{-2}m^{-1}$ was obtained for the x = 0.05 sample, in agreement with the literature report on samples produced on a small scale [5]. Additionally, the electrical transport properties of the x = 0.05 sample were measured repeatedly five times from room temperature to 773 K in a He atmosphere, and the results are shown in Figure 4. It can be seen that the results are very consistent, which is a good indicator of the measurement reliability and also the thermal stability of the sample.

The total thermal conductivity is shown in Figure 3(d). For the undoped TiNiSn sample, the total thermal conductivity (κ) firstly decreased with increasing temperature and then increased above 573 K, which indicates a bipolar effect. But it was suppressed in the samples with Cu addition due to the increased majority carriers. The lattice thermal conductivity (κ_L) was calculated by subtracting the electronic thermal conductivity (κ_e) from κ, with κ_e calculated using the Wiedemann–Franz law, $\kappa_e = LT/\rho$, where L is Lorenz number. L was estimated by using the empirical expression $L = 1.5 + \exp[116/|\alpha|]$ [16]. Due to the sign of the bipolar effect in the undoped TiNiSn sample, the calculated κ_L probably has some contribution from bipolar thermal conduction above 573 K, but this is not critical to the discussion in this work. The calculated κ_L is shown in Figure 3(e), and it can be seen that there was a very obvious reduction of κ_L in the samples with Cu addition. At 323 K, the undoped TiNiSn sample had a κ_L of

5.6 $Wm^{-1}K^{-1}$, which decreased to 4.2 $Wm^{-1}K^{-1}$ for the x = 0.05 sample. It suggests Cu was not only working as a dopant, but produced extra phonon scattering, which is in agreement with the literature [5]. Figure 3(f) shows the temperature dependence of the figure of merit, zT. The zT value was enhanced with Cu addition as a result of an increased power factor and reduced κ_L. A maximum zT value of ~ 0.6 was obtained at 773 K for the x = 0.05 sample, which is 50% higher than that of the undoped TiNiSn. The maximum zT value is very similar to the reported value for TiNiSn-based materials prepared by conventional long duration annealing methods [5, 9, 17]. However, it is much higher than the reported value for TiNiSn-based materials prepared by other unconventional methods [12, 13].

Despite the increased interest in HH compounds, the published reports on their TE modules and performance is sparse. The main challenge in developing high-performance TE modules that can tolerate high temperatures is to develop a good joining method that forms a thermally and mechanically stable joint with low electrical contact resistance (Rc). The impact of Rc on the performance of TE modules with $TiNiCu_{0.05}Sn$ material was evaluated through finite element analysis using COMSOL. This suggested a target value of 1 x 10^{-5} Ωcm^2 for Rc in order to limit the power loss of the TE module to < 5 % due to the contacts. The Rc test assembly for $TiNiCu_{0.05}Sn$ consisted of a uni-junction arrangement of two pellets ($TiNiC_{0.05}Sn$) joined end to end with a joining material and a

metallic contact in the middle. (See Figure S2) This uni-junction design is representative of a junction in an upscaled module, since it includes the complete joining method and thermal history of the joining material. The Rc value was determined using four-point probe resistance measurements at room temperature, along the central axis of the sample, with a spatial resolution of about 50 μm. (See Figure S2) The average Rc measured for eight as built $TiNiCu_{0.05}Sn$ contacts was (2.1 ± 0.3) x 10^{-5} Ωcm^2. The long-term reliability of these contacts was evaluated through isothermal annealing in air at 673 K for 96 hours (Figure 5). There was no obvious increase in both the Rc and the resistivity of the samples during aging. The contacts were mechanically and electrically very good and stable, and close to the target value of 1 x 10^{-5} $\Omega \cdot cm^2$. The variation in Rc was due to the measurement technique and the impact of sample preparation. Although the thermal aging time (96 hours) was relatively short, it indicates good stability of both the contact and the sample. Moreover, to demonstrate up-scaling, a relatively large sample of Φ 30 mm was prepared using the same method. The thermoelectric properties were identical to those of the Φ 15 mm sample (Figure S3). Backscattered SEM images and EDX results (Figure S4) along the cross section of the Φ 30 mm sample indicate that the sample was homogeneous in spite of its large size. The processing route for TiNiSn material in this work is scalable and very promising for thermoelectric module fabrication.

High-quality materials of n-type TiNiSn were successfully synthesised by a fast processing route, which is a combination of AM, BM and SPS. The total synthesis time was about 6 h, which is significantly reduced in comparison with the conventional annealing process (more than a week), and all of the techniques involved are scalable. The purity and homogeneity of the samples (up to Φ 30 mm) were verified by XRD and EDX analysis. With Cu addition, the thermoelectric performance of TiNiSn was largely improved due to enhanced PF and reduced κ_L, and a maximum zT of 0.6 @ 773 K was achieved in $TiNiCu_{0.05}Sn$. This corresponds to the same performance metrics as samples prepared on a small-scale using long annealing times [5]. Preliminary joining and thermal aging tests indicate that a very low Rc of ~ 10^{-5} Ωcm^2 can be achieved and both the joint to copper and sample are stable in air after aging at 673 K for 96 h. This synthesis route opens up the possibility of large-scale production of TiNiSn for thermoelectric module fabrication, and can be extended to other thermoelectric systems.

This work was supported by the Energy Entrepreneurs Fund (ATHLETE).

References

[1] D.M. Rowe, CRC Handbook of Thermoelectrics, CRC Press, 1995.

[2] G.S. Nolas, J. Sharp, H.J. Goldsmid, Thermoelectrics, Springer, Berlin, Heidelberg, 2001.

[3] Z. Tian, S. Lee, G. Chen, Annu. Rev. Heat Transf. 17 (2014) 425-483.

[4] G.J. Tan, L.D. Zhao, M.G. Kanatzidis, Chem. Rev. 116(19) (2016) 12123-12149.

[5] S.A. Barczak, J.E. Halpin, J. Buckman, R. Decourt, M. Pollet, R.I. Smith, D.A. MacLaren, J.-W.G. Bos, ACS Appl. Mater. Interfaces 10(5) (2018) 4786-4793.
[6] G.S. Nolas, J. Poon, M. Kanatzidis, MRS Bull. 31(3) (2006) 199-205.
[7] J.E. Douglas, C.S. Birkel, N. Verma, V.M. Miller, M.-S. Miao, G.D. Stucky, T.M. Pollock, R. Seshadri, J. Appl. Phys. 115(4) (2014) 043720.
[8] R.A. Downie, D.A. MacLaren, R.I. Smith, J.W.G. Bos, Chem. Commun. 49(39) (2013) 4184-4186.
[9] Y. Tang, X. Li, L.H.J. Martin, E. Cuervo Reyes, T. Ivas, C. Leinenbach, S. Anand, M. Peters, G.J. Snyder, C. Battaglia, Energy Environ. Sci. 11(2) (2018) 311-320.
[10] E. Lkhagvasuren, S. Ouardi, G.H. Fecher, G. Auffermann, G. Kreiner, W. Schnelle, C. Felser, AIP Adv. 7(4) (2017) 045010.
[11] A. Karati, B.S. Murty, Mater. Lett. 205 (2017) 114-117.
[12] C.S. Birkel, W.G. Zeier, J.E. Douglas, B.R. Lettiere, C.E. Mills, G. Seward, A. Birkel, M.L. Snedaker, Y. Zhang, G.J. Snyder, T.M. Pollock, R. Seshadri, G.D. Stucky, Chem. Mater. 24(13) (2012) 2558-2565.
[13] M. Zou, J.-F. Li, B. Du, D. Liu, T. Kita, J. Solid State Chem. 182(11) (2009) 3138-3142.
[14] M.M. Zou, J.F. Li, Rare Metal Mater. Eng. 38 (2009) 1079-1082.
[15] M. Tillard, A. Berche, P. Jund, Metals 8(10) (2018) 835.
[16] H.S. Kim, Z.M. Gibbs, Y.L. Tang, H. Wang, G.J. Snyder, APL Mater. 3(4) (2015) 041506.
[17] L. Enkhtaivan, F. Chenguang, H.F. Gerhard, A. Gudrun, K. Guido, S. Walter, F. Claudia, J. Phys. D: Appl. Phys. 50(42) (2017) 425502.

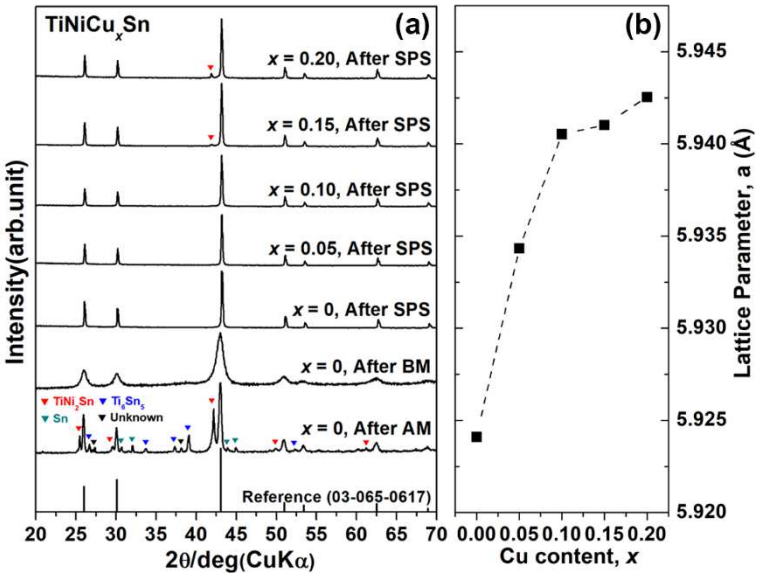

Figure 1. (a) XRD patterns of TiNiCu$_x$Sn (x = 0 ~ 0.2) samples and (b) lattice parameters of TiNiCu$_x$Sn samples after SPS.

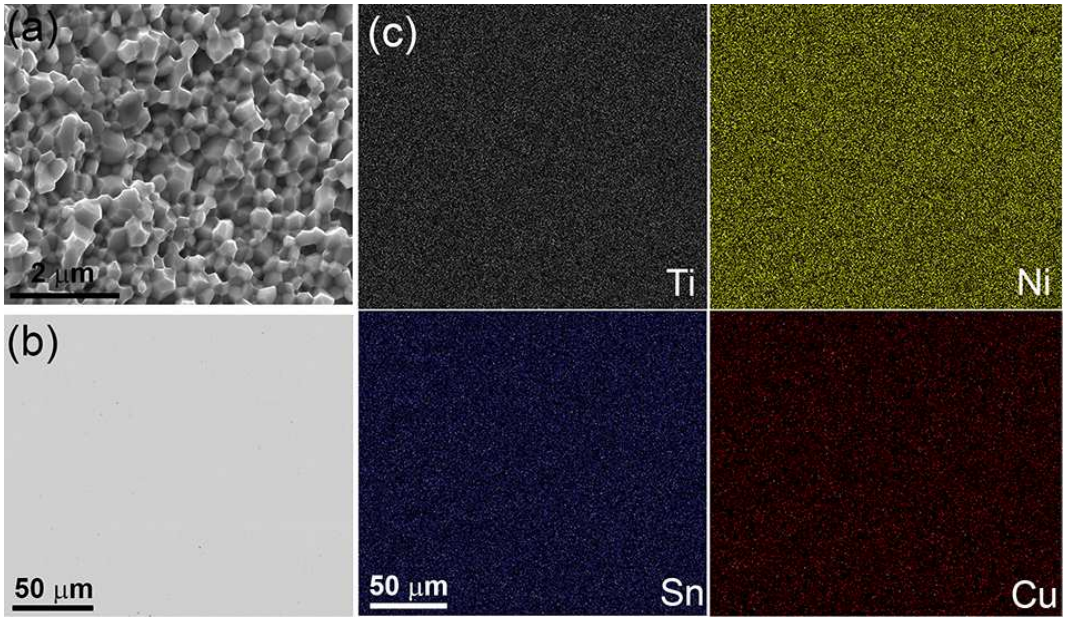

Figure 2. (a) SEM image of fractured surface, (b) Backscattered electron image of polished surface and (c) EDX mapping of polished surface, for a representative sample $TiNiCu_{0.1}Sn$.

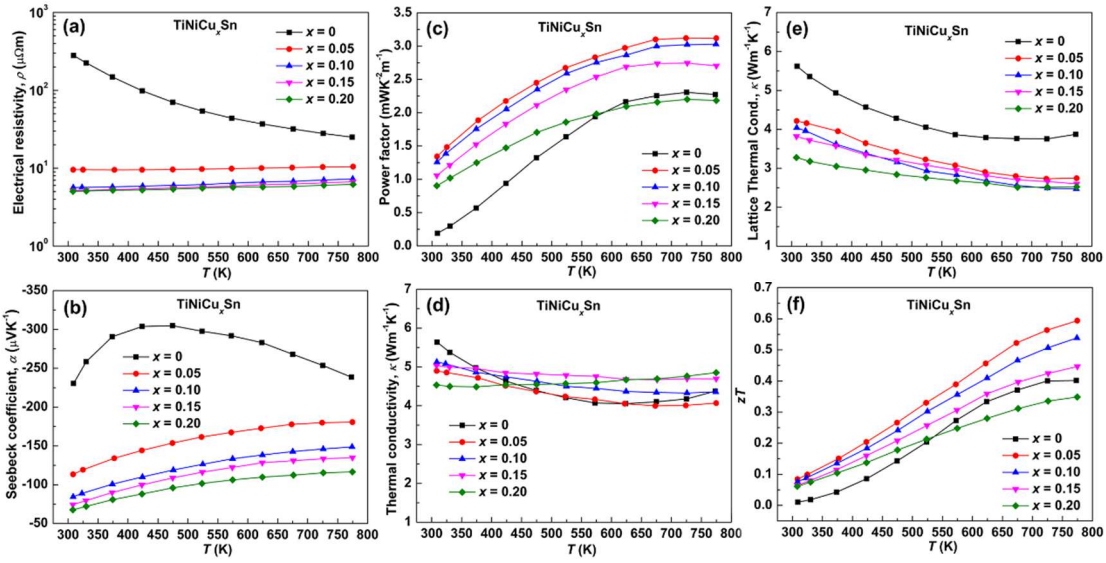

Figure 3. Temperature dependent thermoelectric properties of TiNiCu$_x$Sn (x = 0 ~ 0.2) samples, (a) Electrical resistivity, (b) Seebeck coefficient, (c) Power factor, (d) Thermal conductivity, (e) Lattice thermal conductivity, and (f) Figure of merit, zT.

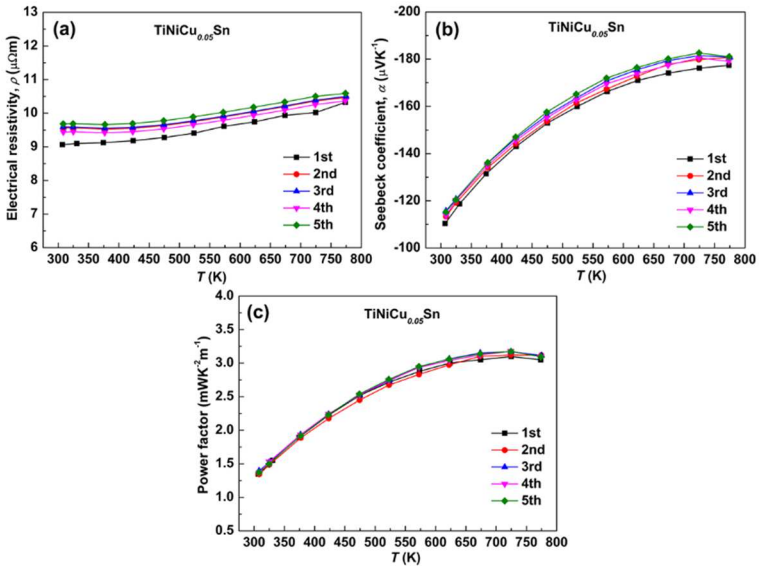

Figure 4. Thermal cycling tests of $TiNiCu_xSn$ (x = 0.05) sample in LSR-3, (a) Electrical resistivity, (b) Seebeck coefficient and (c) Power factor.

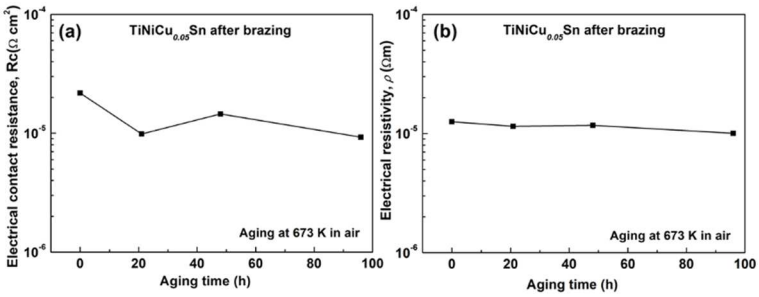

Figure 5. Time dependent (a) electrical contact resistance and (b) electrical resistivity of $TiNiCu_xSn$ (x = 0.05) sample aged at 673 K in air.